Research Article Vol. 31, No. 3 / 30 Jan 2023 / Optics Express 4179
Optics EXPRESS

Complex aspherical singlet and doublet microoptics by grayscale 3D printing

LEANDER SIEGLE,* SIMON RISTOK, AND HARALD GIESSEN

4th Physics Institute and Research Center SCoPE, University of Stuttgart, Pfaffenwaldring 57, 70569 Stuttgart, Germany
l.siegle@pi4.uni-stuttgart.de

Abstract: We demonstrate 3D printed aspherical singlet and doublet microoptical components by grayscale lithography and characterize and evaluate their excellent shape accuracy and optical performance. The typical two-photon polymerization (2PP) 3D printing process creates steps in the structure which is undesired for optical surfaces. We utilize two-photon grayscale lithography (2GL) to create step-free lenses. To showcase the 2GL process, the focusing ability of a spherical and aspherical singlet lens are compared. The surface deviations of the aspherical lens are minimized by an iterative design process and no distinct steps can be measured via confocal microscopy. We design, print, and optimize an air-spaced doublet lens with a diameter of 300 µm. After optimization, the residual shape deviation is less than 100 nm for the top lens and 20 nm for the bottom lens of the doublet. We examine the optical performance with an USAF 1951 resolution test chart to find a resolution of 645 lp/mm.

1. Introduction

From its inception in the 1990's [1–5] 2PP 3D printing became a major microfabrication method as the race for higher resolution [6–11], accuracy [12,13] and eventually size [14–16] solidified its place in research. Given the high flexibility and resolution, the 2PP 3D printing technology serves many fields, e.g. photonic crystals [17–19], metamaterials [20–25], waveguides [26], biological cell-scaffolds [27–29], micro-needles and -fluidics [30,31], endoscopy [32,33] and the integration of quantum technology [34–37]. One large research field with industrial applications is the area of microoptics [38–41]. Here freeform optics [42–45], stacked lenses [46,47] as well as lens arrays [48–51] give the opportunity for high resolution cameras in a previously unreachable size-range. 3D printing is a highly versatile manufacturing method, which generally has no design limits. This is especially important and helpful for 3D printing optical components [41,52], as a larger number of parameters can be varied in the lens design, allowing for simple aspherical lenses or complex multi freeform optics, as described in [42–47] and this publication. All structures are printed in a single step, where no alignment is required. The design process starts with the material parameters, especially the refractive index and dispersion [53,54]. For dimensions, we opt for an outer diameter of 300 µm for all presented optics, with smallest optical features in the tens of micrometre range. Shrinking of the photoresist is compensated via an iterative design process [16], resulting in sub-wavelength shape accuracy required for high optical performance.

2. Fabrication

The 3D printed lenses are fabricated using the commercially available Nanoscribe Quantum X (Nanoscribe GmbH Karlsruhe, Germany) microfabrication system. The printing process is based on two-photon absorption, which is used to polymerize a liquid and transparent photoresist (Nanoscribe IP-S). Ultra-short light pulses at 780 nm are generated by a frequency doubled, amplified Erbium-doped fiber laser and focused by a 25x magnification microscope objective

#480472 https://doi.org/10.1364/OE.480472
Journal © 2023 Received 14 Nov 2022; revised 18 Dec 2022; accepted 31 Dec 2022; published 20 Jan 2023

Optics EXPRESS

with a numerical aperture (NA) of 0.8, creating high light intensities in a small spatial region, in which the photoresist is hardened by two-photon absorption, called a voxel (volume pixel). Arbitrary 3D structures can be created by moving the voxel through the resist. The motion of the voxel is controlled via two galvo mirrors that scan the surface in x- and y-direction. Movement in the z-direction is achieved using a piezoelectric translation stage. The lenses are fabricated in the dip-in laser lithography printing mode: A small drop of the liquid resist is placed on a glass coverslip and the writing objective is subsequently lowered into the resist. This way, focusing of the laser beam is aided by the higher refractive index of the liquid resist, with respect to air. Before applying the liquid resist to the substrate, the glass is cleaned using acetone, isopropyl alcohol, and an oxygen plasma for five minutes, ensuring maximal adhesion.

In this work, two different methods of printing are utilized, combined, and explained in the following. The typical 2PP 3D printing process is schematically shown in Fig. 1(a). A 3D model is first cut into horizontal slices, and each slice is subsequently hatched into parallel hatching lines. The constant sized voxel is then moved along the hatching lines in the slice until it is finished and is then moved upwards to the next slice. This method can create arbitrary 3D structures, but the lens surfaces exhibit small vertical steps of the size of the slicing distance. Reducing the slicing distance decreases the step size at the cost of longer printing times. The second method, namely two-photon grayscale lithography (2GL), provides better shape accuracy when using the same slicing and hatching parameters as the 2PP printing technique by modulating the laser power during the print. Step-free surfaces are manufactured as the power modulation of the laser corresponds to a size modulation of the voxel (Fig. 1(b)). This change in the voxel's size is utilized such that the volume of polymerization matches the designed structure better, leaving no steps measurable by confocal microscopy. Due to the modulation and size adaptation of the voxel to the surface, we can use a larger slicing distance with 2GL compared to 2PP 3D printing and still achieve the desired shape fidelity. A direct comparison between the two techniques for the manufacturing of microoptical components is given in [51]. At the time of writing this paper, 2GL at the Nanoscribe Quantum X only allows for the creation of 2.5D shapes, excluding overhanging parts. Hence, no 3D models are needed for the 2GL process. Instead, a grayscale image is used as a topography map where the grayscale value represents the thickness of the printed areas. The combination of both printing methods is applied in the fabrication of the aspherical doublet. Details are given in the corresponding section below.

A laser scan speed of 200 mm /s is paired with slicing and hatching distances of 1 µm and 0.2 µm, respectively. Furthermore, a multilayer attenuation of 0.8 is chosen for the 2GL printed lenses. This parameter can be adjusted between 0 and 1 and determines the degree of power modulation during fabrication. The supporting structures are printed with the 2PP process, and a hatching angle offset of 90° which is not present for the 2GL structures. Printing times are 7 min for the aspherical focusing lens and 15 min for the doublet. Manufacturing the structures purely with the 2PP printing technique and still achieving similar shape accuracy, we expect these times to increase [51]. After printing, the remaining unpolymerized photoresist is removed by immersing the sample in a developing solution (mr-dev 600, micro resist technology) for 25 min, followed by 5 min in isopropyl alcohol and drying with nitrogen. All optical structures presented in this paper are printed on a 170 µm thick glass substrate.

Optics EXPRESS

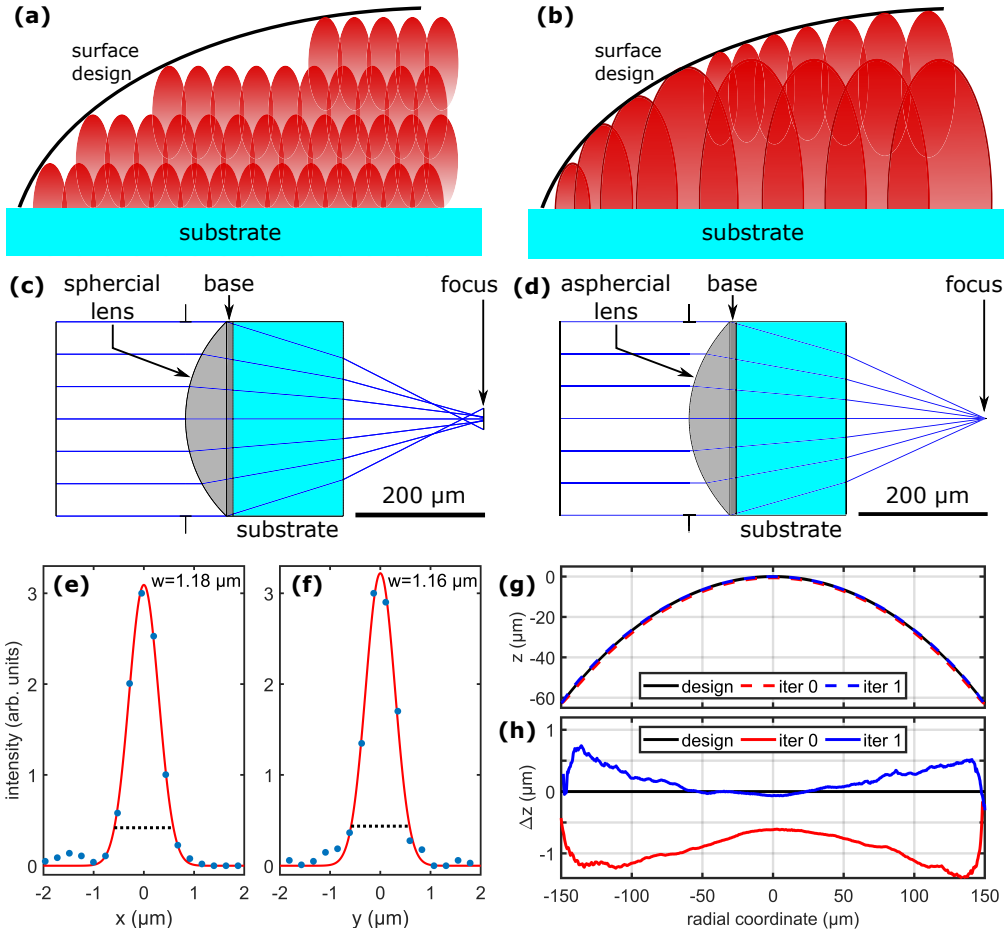

Fig. 1. (a) Schematic of typical voxel position in the two-photon polymerization (2PP) 3D printing process and (b) two-photon grayscale lithography (2GL) 2.5D printing process. Optical designs of the spherical (c) and aspherical (d) focusing lens. Both lenses feature a diameter of 300 µm and a thickness of about 73 µm including the 10 µm thick base. The lens is colored in light gray, the base in dark gray and the substrate is colored light blue. (e) and (f) Beam profiles of the aspherical focus in x- and y-direction, including Gaussian fits in red as well as the $1/e^2$-intensity marked by the black dashed lines. (g) Comparison of the shape of the aspherical design and the print. (h) Deviation profile for the aspherical lens fitted with a polynomial function used in the optimization process. "iter 0" and "iter 1" refer to the unchanged and first iteration of the print.

Optics EXPRESS

3. Spherical and aspherical focusing lens

In this section we give a short overview of the most basic 3D printed optical focusing component, a singlet lens. Both a spherical and aspherical lens with a diameter of 300 µm and a thickness of 63 µm are printed on top of a 10 µm thick base layer with the 2GL process parameters described above. The optical design and ray tracing simulation is performed with ZEMAX OpticsStudio and lenses are illustrated in Fig. 1(c) and (d), respectively. For the aspheric lens we add the term $a_2 \cdot r^2$ to the spherical surface design, where r is the radius of the lens, and $a_2 = 0.6383\,\mathrm{mm}^{-1}$ determined by OpticsStudio to achieve a smaller focus spot compared to the spherical lens.

The focusing ability at the focal length of 217 µm is compared by fitting Gaussian functions through the intensity in the focal plane. We determine the $1/e^2$-intensity width w to be 1.61 µm and 1.65 µm for the spherical lens in x- and y-direction, respectively. For the aspherical lens we measure 1.18 µm and 1.16 µm (Fig. 1(e) and (f)). Here, the dotted lines show the $1/e^2$-intensity width. The simulations give values of w=1.13 µm for the spherical lens and 0.98 µm for the aspherical one, providing just slightly smaller values than the measurements.

A comparison of the printed aspherical lens with respect to the design is given in Fig. 1(g) and (h). Here "iter 0" and "iter 1" refer to the printing of the original design and the printing of the first iterated design, respectively. As the printed structure deviates from the desired shape by more than 500 nm, we create an adapted design which precompensates the measured deviations. A polynomial fit of 12th order is fitted to the measured profile and the deviation from the design is determined and subsequently added to the original design. This is the first iterated design, where the profiles are also illustrated in Fig. 1(g) and (h). The deviations of this first iteration are reduced over the entire lens profile and only surpass 500 nm towards the outside of the lens. This method of iterating the design of a structure via topography measurements is a very powerful technique that will be used more in the following section.

As the slicing distance is 1 µm, one would expect steps of the same size with the typical 2PP process. Due to the 2GL process, no such steps are visible in the profiles illustrated in Fig. 1(g) and (h), which signifies the excellent use case for optical elements. We expect fewer optical losses due to less scattering and a better wave front accuracy. The optical performance is discussed in the upcoming example of the air-spaced doublet lens. All lens surfaces are measured with a confocal microscope (nanofocus µsurf expert) using a 50x magnification objective with an NA of 0.95.

4. Air-spaced doublet

Focusing optical systems only require few optically active surfaces, e.g., an aspherical singlet lens as described above. Optical imaging requires more sophisticated designs including more optically active surfaces. In this section, we describe and explain the design, analyze the shape, and examine the optical performance of an air-spaced doublet containing two aspherical lenses.

4.1. Design

The design of the optically active surfaces of the air-spaced doublet created with the software ZEMAX OpticsStudio is shown in Fig. 2(a). Parallel rays coming from an object infinitely far away from the lens system are transmitted through the 170 µm thick glass substrate and strike an aperture with a diameter of 100 µm at the end of the substrate before travelling into the bottom lens. The bottom lens is used to widen the beam paths to allow an optimization of the top lens based on the different field angles of up to 30°, allowing for a designed field of view of 60°. Both lenses have a flat bottom and an aspherically curved top surface, owing to the 2.5D limitation of the 2GL process (no overhanging surfaces). The focal length of the system is 275 µm, with an f-number of 3.181 and an NA of 0.154. The two lenses have a ring of constant thickness around the optically active aspherical surface, which is used to anchor the top lens to the substrate

Optics EXPRESS

(Fig. 2(b) and (c)). For the bottom lens, the ring of constant thickness serves as an aid for measuring the important optically active surface and also to reduce shape deviations which are usually largest at the edges of the lens, see e.g. [16]. The optically active surfaces of the lenses have diameters of 114 µm and 243 µm, respectively, and the entire optical system has a total diameter of 300 µm and a total thickness of 197 µm. As there is an air gap between the bottom and top lens, we introduce supporting structures which connect the lens to the glass substrate (Fig. 3(a)). It consists of eight pillars connected by two rings at the ends for optimal adhesion to the substrate and the lens and increased mechanical stability. Gaps in the design are required to remove the unpolymerized photoresist during the developing process. A second supporting structure (bottom of Fig. 3(a)) is used as an aid for the aperture stop and placed directly below the bottom lens. It is designed as a truncated cone with the base diameter of 100 µm matching that of the aperture. This serves as a reference while adjusting the iris diaphragm of the optical microscopy setup used for the characterization of the optical performance, as described below.

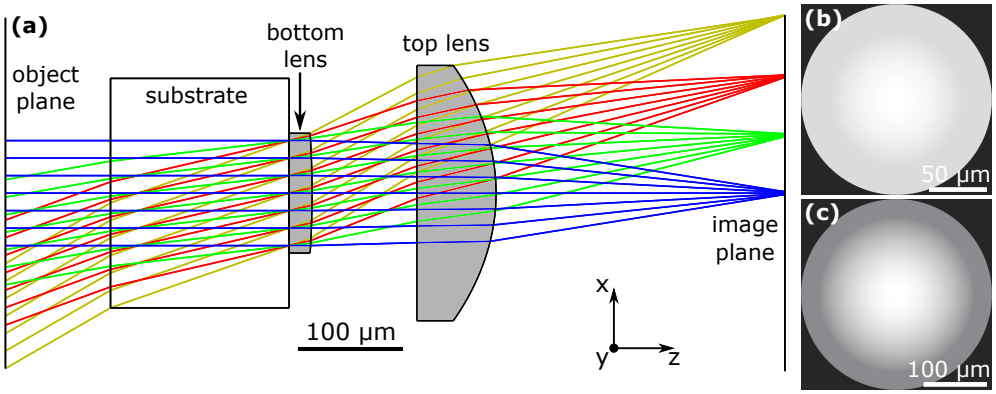

Fig. 2. Optical design of the air-spaced doublet. (a) Optical beam path through the lens system, differently colored rays indicate the various field angles (0° to 30° in 10° steps). (b) and (c) Grayscale images of the aspherical bottom and top lens, respectively.

4.2. Shape analysis and correction

To illustrate the shape of the lens surfaces of the air-spaced doublet, we printed a 3/4 version of the structure, enabling the investigation of the inside, e.g., by using a scanning electron microscope (Fig. 3(b)). The surfaces of the two lenses are smooth and do not show steps or other types of misstructuring. The two small images below illustrate zoom-ins of the original structure at higher resolution. The different writing modes can be distinguished in the bottom right image (Fig. 3(b)), where the bottom is printed with the typical 2PP process and shows steps in z-direction, and the top part is printed by the 2GL process without any steps. Especially the image on the left illustrates the usage of an 90° hatching offset angle in the 2PP process as well as the slicing distance of 1 µm.

A sample overview of five air-spaced doublets is given in Fig. 3(c). The structures are clear with smooth surfaces, indicating the high repeatability of the fabrication process.

The shape of both lenses is optimized using the iterative design process described before. We use the difference between the measured profile and the design to create a new design which is subsequently printed as the first iteration. This process is then repeated. To create the design of the second iteration, we add the difference of the original design and the measured profile of the first iteration to the design of the first iteration.

The results of the iterative optimization process are illustrated in Fig. 3(d) and (e), indicating the deviations from design for the bottom and top lens. The surface of the bottom lens initially

Optics EXPRESS

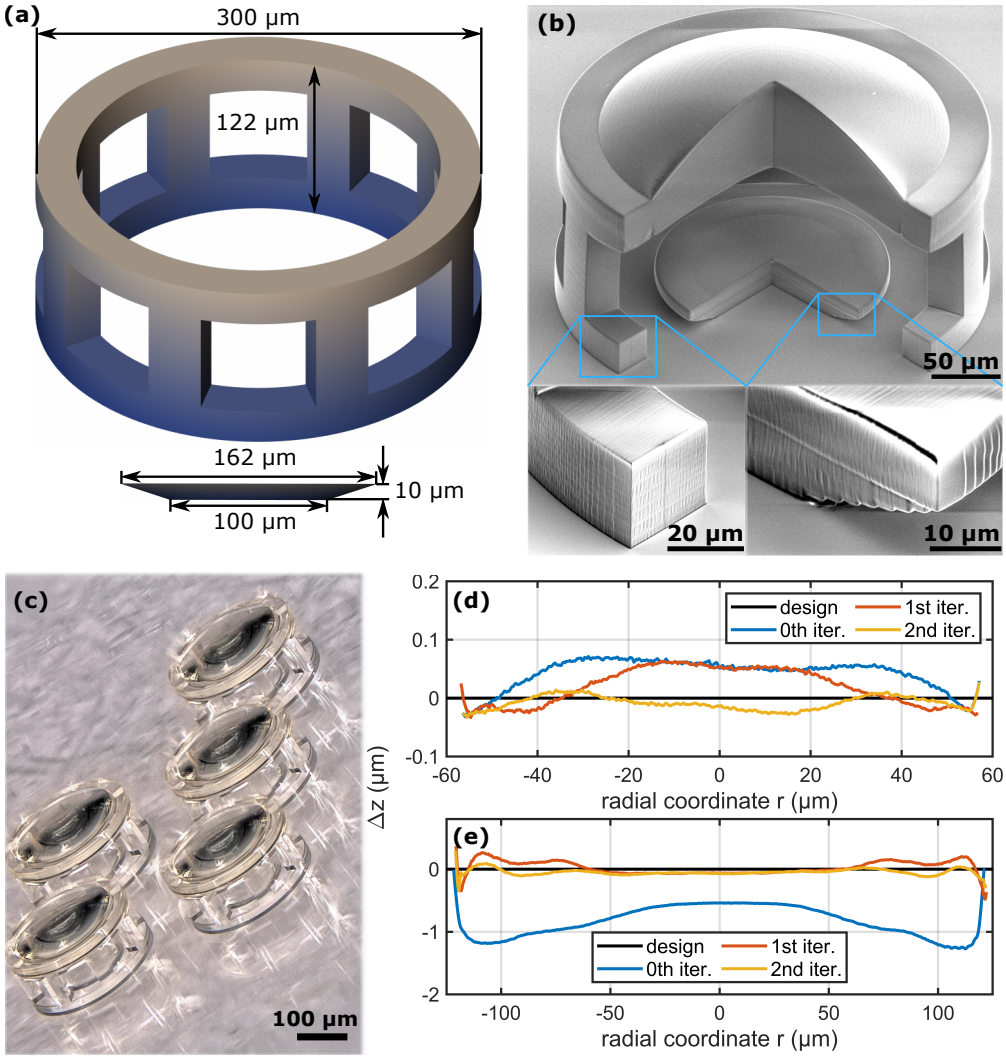

Fig. 3. 3D printed air-spaced doublet. (a) Design of the supporting structures for the top lens as well as side view of the designed base structure below the bottom lens. (b) Scanning electron microscope image of an air-spaced doublet, which has been printed with one quarter cut out to better illustrate the internal structure. Zoom-ins for the supporting structure of the top lens and the bottom lens are illustrated below. (c) Optical image of five air-spaced doublets. (d) and (e): Deviations with respect to the design of the zeroth, first, and second iteration, both for the bottom lens (d) and the top lens (e), mind the different scaling of the x-axis.

Optics EXPRESS

deviated up to 70 nm for the desired shape, which could be reduced to below 20 nm after two iterations. For the top lens, the original structure exhibits shape deviations of 0.5 µm in the center, increasing to about 1.2 µm at the edge of the lens (Fig. 3(e)). The first iteration eliminates most of the deviations in the center but still shows larger deviations at the edge of the lens, which is improved in the second iteration. The remaining deviations in the main region of the lens are below 0.1 µm, only increasing to higher values in the outmost part close to the edge. We also measured the spatial root mean square roughness Sq for both lenses, they typically range from 4 nm to 15 nm.

4.3. Optical performance

We examine the optical performance of the air-spaced doublet. The microscopy setup used for imaging characterization is sketched in Fig. 4(a) and already described previously [16]. A diffusor plate is illuminated by a white LED which is collimated by an achromatic lens. This allows a homogeneous intensity distribution to enter the following setup. The light is subsequently focused by a microscope objective onto the air-spaced doublet. The transmitted light is collected by a second objective and is focused by a tube lens onto the CMOS sensor. We place a USAF 1951 resolution test chart between the first objective and the air-spaced doublet. To simulate an aperture stop, an iris diaphragm with adjustable diameter is inserted into the beam path. The diameter and position are chosen such that a sharp image of the iris is projected onto the bottom of the supporting structure of the bottom lens and matches the designed aperture stop diameter of 100 µm.

The imaging quality of the air-spaced doublet can be examined by the different groups of the resolution test chart illustrated in Fig. 4(b) through (g). To achieve higher magnification images, the object distance between the target and the air-spaced doublet is reduced. Figure 4(b) illustrates the lowest magnification and shows high sharpness and contrast. The observed barrel distortion and small chromatic aberrations are expected, as the air-spaced doublet is only designed for a wavelength of 550 nm and made from a single material. The barrel distortion is reduced in the higher magnifications of the target illustrated in Fig. 4(c) through (e), showing groups 2 and 3, 4 and 5 as well as 6 and 7. Here, we observe high contrast and sharpness, though the test chart is out of focus at the edge of the image. For groups 6 and 7, the image is undistorted, and no large aberrations are observed. The air-spaced doublet can resolve the highest group numbers of the target, namely 8 and 9, given in Fig. 4(f). Here, the contrast is not as strong as for smaller magnifications and a blue hue covers the image, which might be caused by stray light. A cut-out of group 9 is given in Fig. 4(g) and shows the excellent resolution of the air-spaced doublet, corresponding to a resolution of 645 lp /mm, where the lines have a width of 0.775 µm. Commercially available USAF 1951 resolution test charts are only available up to number 3 of group 9, which can still be resolved, underlining the optical power of the presented doublet. The measurements illustrate the excellent optical performance and quality of the air-spaced doublet.

Optics EXPRESS

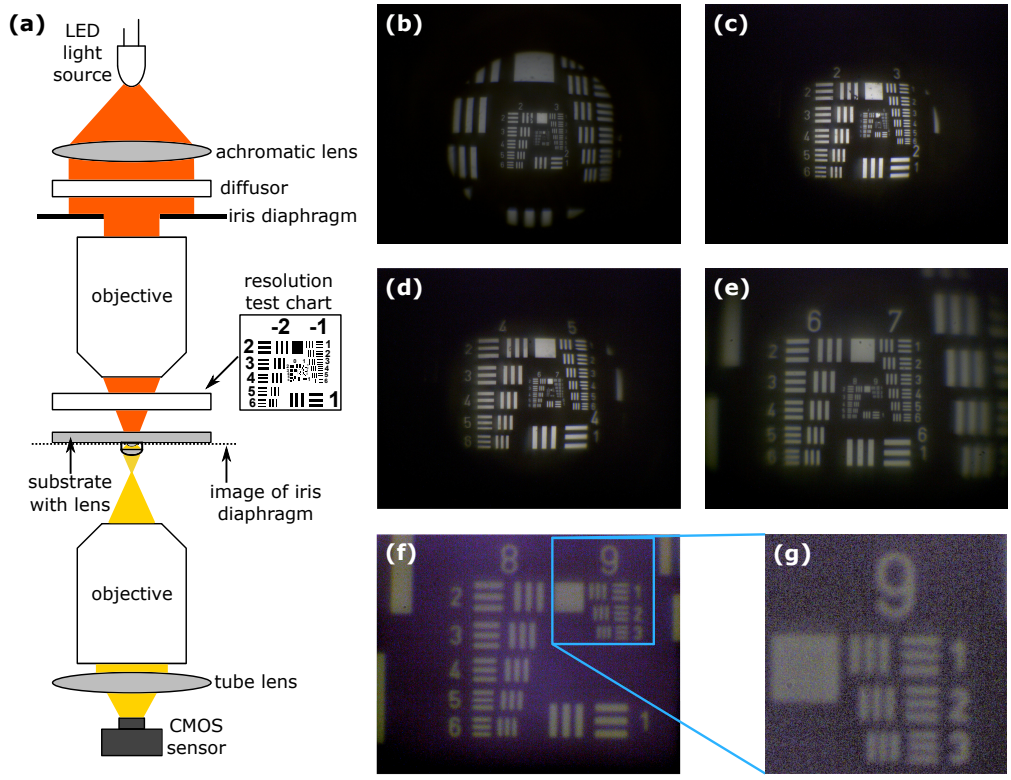

Fig. 4. Imaging performance of the air-spaced doublet. (a) Optical microscope setup to test imaging performance, as previously used in [16]. (b)-(f) Different magnifications of the USAF 1951 resolution test chart, starting from the inner lines of group 0 and 1 in (b) and going to group 8 and 9 in (f). (g) Zoom-in of (f), displaying the smallest elements of group 9 of the chart, corresponding to a resolution of 645 lp /mm. (b)-(f) have the same size on the camera sensor.

5. Conclusion and outlook

We presented the design, fabrication, and optimization of multiple microoptical elements. The spherical and aspherical singlet lenses highlight the step-free printing by the means of the two-photon grayscale lithography process. Here, the focusing ability matches the expectations, and deviations of the surface shape are corrected by means of an iterative design process. Moreover, we designed an air-spaced doublet with a field of view of 60°, which showed excellent shape accuracy and optical performance. The iterative design process to correct shrinking of the photoresist leaves only minor deviations from the desired shape, namely less than 20 nm for the bottom lens and 100 nm for the larger top top lens. The spatial root mean square roughness Sq was as small as 4 nm. The air-spaced doublet boasts excellent optical performance with high sharpness and resolution up to 645 lp /mm in the center of the image. Combining the high shape accuracy and small surface roughness with the high resolution shows the power of the 2GL printing method for microoptical components. In this study we have not taken the local change of refractive index into account, which comes about if different laser powers are used during the printing process [55]. Although it should only play a minor role for refractive microoptical components, as the slicing distances are very small, understanding and studying this change could further push the optical capabilities and give more degrees of freedom to the designer. As more complex optical designs implement a higher number of reflective surfaces,

Optics EXPRESS

anti-reflective coatings [56] or structured surfaces [57] can be used to reduce reflective losses. In the future, multiple materials could be printed with the two-photon grayscale lithography process, allowing even more flexible parameters and complex designs like an achromat and apochromat [58]. Especially for applications in quantum technology, such as coupling 3D printed cavities to single photon emitters, grayscale lithography can improve existing designs [59,60].

Funding. Carl-Zeiss-Stiftung (EndoPrint3D); Baden-Württemberg Stiftung (OPTERIAL); Ministerium für Wissenschaft, Forschung und Kunst Baden-Württemberg (Innovation Campus Future Mobility: SdManu1); Bundesministerium für Bildung und Forschung (PRINTOPTICS, QLink.X, QR.X); Deutsche Forschungsgemeinschaft (DFG-UP31/1, GRK 2642); HORIZON EUROPE European Research Council (3DPRINTEDOPTICS: 862549).

Disclosures. The authors declare no conflicts of interest.

Data Availability. Data underlying the results presented in this paper are not publicly available at this time but may be obtained from the authors upon reasonable request.

References

1. J. H. Strickler and W. W. Webb, *Two-photon excitation in laser scanning fluorescence microscopy* (SPIE, 1991), p. 107–118.
2. E.-S. Wu, J. H. Strickler, W. R. Harrell, and W. W. Webb, *Two-photon lithography for microelectronic application*, (SPIE, 1992), p. 776–782.
3. S. Maruo, O. Nakamura, and S. Kawata, "Three-dimensional microfabrication with two-photon-absorbed photopolymerization," Opt. Lett. **22**(2), 132–134 (1997).
4. S. Maruo and S. Kawata, "Two-photon-absorbed near-infrared photopolymerization for three-dimensional microfabrication," J. Microelectromech. Syst. **7**(4), 411–415 (1998).
5. H.-B. Sun, S. Matsuo, and H. Misawa, "Three-dimensional photonic crystal structures achieved with two-photon-absorption photopolymerization of resin," Appl. Phys. Lett. **74**(6), 786–788 (1999).
6. S. Kawata, H.-B. Sun, T. Tanaka, and K. Takada, "Finer features for functional microdevices," Nature **412**(6848), 697–698 (2001).
7. R. J. DeVoe, H. W. Kalweit, C. A. Leatherdale, and T. R. Williams, *Voxel shapes in two-photon microfabrication* (SPIE, 2003), p. 310–316.
8. H.-B. Sun and S. Kawata, *Two-Photon Photopolymerization and 3D Lithographic Microfabrication* (Springer, 2004), pp. 169–273.
9. A. Spangenberg, N. Hobeika, F. Stehlin, J.-P. Malval, F. Wieder, P. Prabhakaran, P. Baldeck, and O. Soppera, *Recent Advances in Two-Photon Stereolithography* (IntechOpen, 2013).
10. J. Fischer and M. Wegener, "Three-dimensional optical laser lithography beyond the diffraction limit," Laser Photonics Rev. **7**(1), 22–44 (2013).
11. Z. Gan, Y. Cao, R. A. Evans, and M. Gu, "Three-dimensional deep sub-diffraction optical beam lithography with 9 nm feature size," Nat. Commun. **4**(1), 2061 (2013).
12. X. Zhou, Y. Hou, and J. Lin, "A review on the processing accuracy of two-photon polymerization," AIP Adv. **5**(3), 030701 (2015).
13. G. Dai, X. Hu, J. Hering, M. Eifler, J. Seewig, and G. von Freymann, "Define and measure the dimensional accuracy of two-photon laser lithography based on its instrument transfer function," JPhys Photonics **3**(3), 34002 (2021).
14. L. Jonušauskas, S. Juodkazis, and M. Malinauskas, "Optical 3d printing: bridging the gaps in the mesoscale," J. Opt. **20**(5), 053001 (2018).
15. L. Jonušauskas, D. Gailevicius, S. Rekštyte, T. Baldacchini, S. Juodkazis, and M. Malinauskas, "Mesoscale laser 3d printing," Opt. Express **27**(11), 15205–15221 (2019).
16. S. Ristok, S. Thiele, A. Toulouse, A. M. Herkommer, and H. Giessen, "Stitching-free 3d printing of millimeter-sized highly transparent spherical and aspherical optical components," Opt. Mater. Express **10**(10), 2370–2378 (2020).
17. M. Deubel, G. von Freymann, M. Wegener, S. Pereira, K. Busch, and C. M. Soukoulis, "Direct laser writing of three-dimensional photonic-crystal templates for telecommunications," Nat. Mater. **3**(7), 444–447 (2004).
18. M. Thiel, G. von Freymann, and M. Wegener, "Layer-by-layer three-dimensional chiral photonic crystals," Opt. Lett. **32**(17), 2547–2549 (2007).
19. Y. Liu, H. Wang, J. Ho, R. C. Ng, R. J. H. Ng, V. H. Hall-Chen, E. H. H. Koay, Z. Dong, H. Liu, C.-W. Qiu, J. R. Greer, and J. K. W. Yang, "Structural color three-dimensional printing by shrinking photonic crystals," Nat. Commun. **10**(1), 4340 (2019).
20. M. S. Rill, C. Plet, M. Thiel, I. Staude, G. von Freymann, S. Linden, and M. Wegener, "Photonic metamaterials by direct laser writing and silver chemical vapour deposition," Nat. Mater. **7**(7), 543–546 (2008).
21. M. S. Rill, C. E. Kriegler, M. Thiel, G. von Freymann, S. Linden, and M. Wegener, "Negative-index bianisotropic photonic metamaterial fabricated by direct laser writing and silver shadow evaporation," Opt. Lett. **34**(1), 19–21 (2009).
22. T. Bückmann, N. Stenger, M. Kadic, J. Kaschke, A. Frölich, T. Kennerknecht, C. Eberl, M. Thiel, and M. Wegener, "Tailored 3d mechanical metamaterials made by dip-in direct-laser-writing optical lithography," Adv. Mater. **24**(20), 2710–2714 (2012).

Optics EXPRESS

23. J. Qu, M. Kadic, and M. Wegener, "Three-dimensional poroelastic metamaterials with extremely negative or positive effective static volume compressibility," Extrem. Mech. Lett. **22**, 165–171 (2018).
24. V. Hahn, P. Kiefer, T. Frenzel, J. Qu, E. Blasco, C. Barner-Kowollik, and M. Wegener, "Rapid assembly of small materials building blocks (voxels) into large functional 3d metamaterials," Adv. Funct. Mater. **30**(26), 1907795 (2020).
25. G. E. Lio, A. Ferraro, T. Ritacco, D. M. Aceti, A. D. Luca, M. Giocondo, and R. Caputo, "Leveraging on enz metamaterials to achieve 2d and 3d hyper-resolution in two-photon direct laser writing," Adv. Mater. **33**(18), 2008644 (2021).
26. A. Bertoncini and C. Liberale, "3d printed waveguides based on photonic crystal fiber designs for complex fiber-end photonic devices," Optica **7**(11), 1487–1494 (2020).
27. M. Malinauskas, S. Rekštyte, L. Lukoševicius, S. Butkus, E. Balciunas, M. Peciukaityte, D. Baltriukiene, V. Bukelskiene, A. Butkevicius, P. Kucevicius, V. Rutkunas, and S. Juodkazis, "3d microporous scaffolds manufactured via combination of fused filament fabrication and direct laser writing ablation," Micromachines **5**(4), 839–858 (2014).
28. J. K. Hohmann and G. von Freymann, "Influence of direct laser written 3d topographies on proliferation and differentiation of osteoblast-like cells: Towards improved implant surfaces," Adv. Funct. Mater. **24**(42), 6573–6580 (2014).
29. A. Erben, M. Hörning, B. Hartmann, T. Becke, S. A. Eisler, A. Southan, S. Cranz, O. Hayden, N. Kneidinger, M. Königshoff, M. Lindner, G. E. M. Tovar, G. Burgstaller, H. Clausen-Schaumann, S. Sudhop, and M. Heymann, "Precision 3d-printed cell scaffolds mimicking native tissue composition and mechanics," Adv. Healthcare Mater. **9**(24), 2000918 (2020).
30. M. Kavaldzhiev, J. E. Perez, Y. Ivanov, A. Bertoncini, C. Liberale, and J. Kosel, "Biocompatible 3d printed magnetic micro needles," Biomed. Phys. Eng. Express **3**(2), 025005 (2017).
31. S. Bohne, M. Heymann, H. N. Chapman, H. K. Trieu, and S. Bajt, "3d printed nozzles on a silicon fluidic chip," Rev. Sci. Instrum. **90**(3), 035108 (2019).
32. J. Li, S. Thiele, B. C. Quirk, R. W. Kirk, J. W. Verjans, E. Akers, C. A. Bursill, S. J. Nicholls, A. M. Herkommer, H. Giessen, and R. A. McLaughlin, "Ultrathin monolithic 3d printed optical coherence tomography endoscopy for preclinical and clinical use," Light: Sci. Appl. **9**(1), 124 (2020).
33. S. Sivankutty, A. Bertoncini, V. Tsvirkun, N. G. Kumar, G. Brévalle, G. Bouwmans, E. R. Andresen, C. Liberale, and H. Rigneault, "Miniature 120-beam coherent combiner with 3d-printed optics for multicore fiber-based endoscopy," Opt. Lett. **46**(19), 4968–4971 (2021).
34. S. Fischbach, A. Schlehahn, A. Thoma, N. Srocka, T. Gissibl, S. Ristok, S. Thiele, A. Kaganskiy, A. Strittmatter, T. Heindel, S. Rodt, A. Herkommer, H. Giessen, and S. Reitzenstein, "Single quantum dot with microlens and 3d-printed micro-objective as integrated bright single-photon source," ACS Photonics **4**(6), 1327–1332 (2017).
35. A. Landowski, J. Gutsche, S. Guckenbiehl, M. Schönberg, G. von Freymann, and A. Widera, "Coherent remote control of quantum emitters embedded in polymer waveguides," APL Photonics **5**(1), 016101 (2020).
36. L. Bremer, K. Weber, S. Fischbach, S. Thiele, M. Schmidt, A. Kaganskiy, S. Rodt, A. Herkommer, M. Sartison, S. L. Portalupi, P. Michler, H. Giessen, and S. Reitzenstein, "Quantum dot single-photon emission coupled into single-mode fibers with 3d printed micro-objectives," APL Photonics **5**(10), 106101 (2020).
37. P. Ruchka, S. Hammer, M. Rockenhäuser, R. Albrecht, J. Drozella, S. Thiele, H. Giessen, and T. Langen, "Microscopic 3d printed optical tweezers for atomic quantum technology," Quantum Sci. Technol. **7**(4), 045011 (2022).
38. K. Sugioka and Y. Cheng, "Femtosecond laser three-dimensional micro- and nanofabrication," Appl. Phys. Rev. **1**(4), 041303 (2014).
39. J. K. Hohmann, M. Renner, E. H. Waller, and G. von Freymann, "Three-dimensional μ-printing: An enabling technology," Adv. Opt. Mater. **3**(11), 1488–1507 (2015).
40. M. Malinauskas, A. Žukauskas, S. Hasegawa, Y. Hayasaki, V. Mizeikis, R. Buividas, and S. Juodkazis, "Ultrafast laser processing of materials: from science to industry," Light: Sci. Appl. **5**(8), e16133 (2016).
41. D. Gonzalez-Hernandez, S. Varapnickas, A. Bertoncini, C. Liberale, and M. Malinauskas, "Micro-optics 3d printed via multi-photon laser lithography," Adv. Opt. Mater. p. 2201701 (2022).
42. R. Guo, S. Xiao, X. Zhai, J. Li, A. Xia, and W. Huang, "Micro lens fabrication by means of femtosecond two photon photopolymerization," Opt. Express **14**(2), 810–816 (2006).
43. T. Gissibl, S. Thiele, A. Herkommer, and H. Giessen, "Sub-micrometre accurate free-form optics by three-dimensional printing on single-mode fibres," Nat. Commun. **7**(1), 11763 (2016).
44. L. Jonušauskas, D. Gailevicius, L. Mikoliunaite, D. Sakalauskas, S. Šakirzanovas, S. Juodkazis, and M. Malinauskas, "Optically clear and resilient free-form μ-optics 3d-printed via ultrafast laser lithography," Materials **10**(1), 12 (2017).
45. A. Bertoncini, S. P. Laptenok, L. Genchi, V. P. Rajamanickam, and C. Liberale, "3d-printed high-na catadioptric thin lens for suppression of xpm background in stimulated raman scattering microscopy," J. Biophotonics **14**(5), e202000219 (2021).
46. T. Gissibl, S. Thiele, A. Herkommer, and H. Giessen, "Two-photon direct laser writing of ultracompact multi-lens objectives," Nat. Photonics **10**(8), 554–560 (2016).
47. S. Thiele, C. Pruss, A. M. Herkommer, and H. Giessen, "3d printed stacked diffractive microlenses," Opt. Express **27**(24), 35621–35630 (2019).

Optics EXPRESS

48. F. C. Wippermann, D. Radtke, U. Zeitner, J. W. Duparré, A. Tünnermann, M. Amberg, S. Sinzinger, C. Reinhardt, A. Ovsianikov, and B. N. Chichkov, *Fabrication technologies for chirped refractive microlens arrays*, (SPIE, 2006), p. 62880O.
49. A. Žukauskas, M. Malinauskas, C. Reinhardt, B. N. Chichkov, and R. Gadonas, "Closely packed hexagonal conical microlens array fabricated by direct laser photopolymerization," Appl. Opt. **51**(21), 4995–5003 (2012).
50. D. Schäffner, T. Preuschoff, S. Ristok, L. Brozio, M. Schlosser, H. Giessen, and G. Birkl, "Arrays of individually controllable optical tweezers based on 3d-printed microlens arrays," Opt. Express **28**(6), 8640–8645 (2020).
51. T. Aderneuer, O. Fernández, and R. Ferrini, "Two-photon grayscale lithography for free-form micro-optical arrays," Opt. Express **29**(24), 39511 (2021).
52. A. Heinrich, *3D Printing of Optical Components*, vol. 233 (Springer International Publishing, 2021, Ch. 6).
53. T. Gissibl, S. Wagner, J. Sykora, M. Schmid, and H. Giessen, "Refractive index measurements of photo-resists for three-dimensional direct laser writing," Opt. Mater. Express **7**(7), 2293–2298 (2017).
54. M. Schmid, D. Ludescher, and H. Giessen, "Optical properties of photoresists for femtosecond 3d printing: refractive index, extinction, luminescence-dose dependence, aging, heat treatment and comparison between 1-photon and 2-photon exposure," Opt. Mater. Express **9**(12), 4564–4577 (2019).
55. A. Žukauskas, I. Matulaitiene, D. Paipulas, G. Niaura, M. Malinauskas, and R. Gadonas, "Tuning the refractive index in 3d direct laser writing lithography: towards grin microoptics," Laser Photonics Rev. **9**(6), 706–712 (2015).
56. S. Ristok, P. Flad, and H. Giessen, "Atomic layer deposition of conformal anti-reflective coatings on complex 3d printed micro-optical systems," Opt. Mater. Express **12**(5), 2063–2071 (2022).
57. Y. Li, D. B. Fullager, E. Angelbello, D. Childers, G. Boreman, and T. Hofmann, "Broadband near-infrared antireflection coatings fabricated by three-dimensional direct laser writing," Opt. Lett. **43**(2), 239–242 (2018).
58. M. Schmid, F. Sterl, S. Thiele, A. Herkommer, and H. Giessen, "3d printed hybrid refractive/diffractive achromat and apochromat for the visible wavelength range," Opt. Lett. **46**(10), 2485–2488 (2021).
59. L. Kohler, M. Mader, C. Kern, M. Wegener, and D. Hunger, "Tracking brownian motion in three dimensions and characterization of individual nanoparticles using a fiber-based high-finesse microcavity," Nat. Commun. **12**(1), 6385 (2021).
60. J. Hessenhauer, K. Weber, J. Benedikter, T. Gissibl, J. Höfer, H. Giessen, and D. Hunger, "Laser written mirror profiles for open-access 2 fabry-pérot microcavities," submitted (2022).